

Detection of quantum spin liquid by probing QSL/normal metal heterostructure with external noise

Priyanka Mondal¹ and Branislav K. Nikolić^{1,*}

¹Department of Physics and Astronomy, University of Delaware, Newark, DE 19716, USA

Abstract

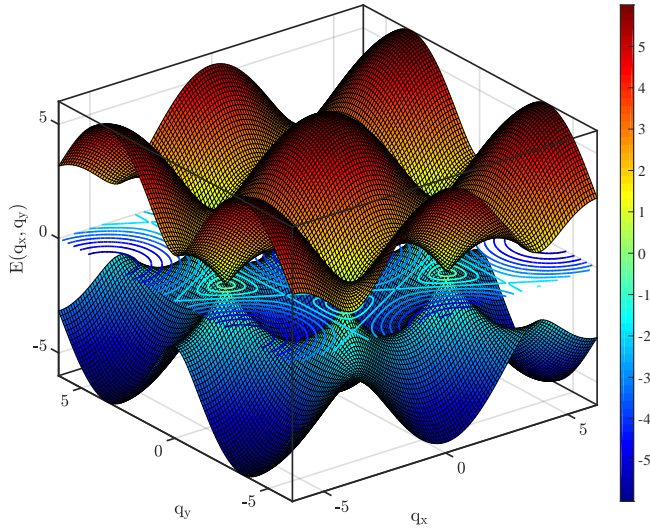


FIG. 1. Energy spectra of matter fermions in ref to [1] in gapless phase i.e. $J_x = J_y = J_z = \frac{1}{3}$. Ground state energy dispersion of the Kitaev Hamiltonian exhibits Dirac cones similar to fermions hopping in graphene.

I. INTRODUCTION

The kitaev Hamiltonian is given by,

$$H = -J_x \sum_{\langle ij \rangle_x} \sigma_i^x \sigma_j^x - J_y \sum_{\langle ij \rangle_y} \sigma_i^y \sigma_j^y - J_z \sum_{\langle ij \rangle_z} \sigma_i^z \sigma_j^z \quad (1)$$

The ground state excitation spectra for the above Hamiltonian is given by,

$$E(\mathbf{q}) = 2|S(\mathbf{q})| \quad (2)$$

where $S(\mathbf{q}) = \sum_{\mathbf{n}_i} J_{\alpha(\mathbf{n}_i)} e^{i\mathbf{qn}_i}$ with $\alpha = x, y, z$ and $\mathbf{n}_0 = \mathbf{n}_z = (0, 0)$, $\mathbf{n}_1 = \mathbf{n}_x = \frac{1}{2}(1, \sqrt{3})$, $\mathbf{n}_2 = \mathbf{n}_y = \frac{1}{2}(-1, \sqrt{3})$.

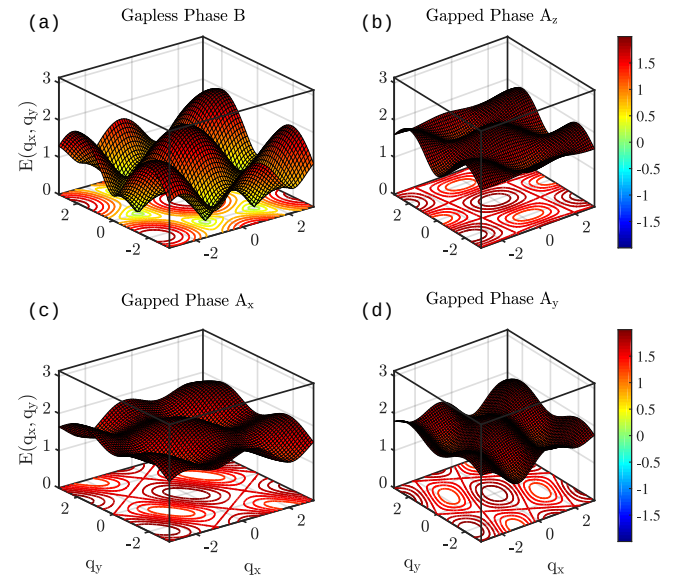


FIG. 2. Energy spectra of matter fermions in ref to [1]. Panel (a) shows energy spectra for gapless phase B where $J_x = J_y = J_z = \frac{1}{3}$ eV. It has behavior similar to fermions in graphene lattice structure with appearance of Dirac cones within first Brillouin zone obtained from exact solution of Kitaev Hamiltonian using Majorana fermions. Panel (a) shows the gapped phase A_z with $J_x = J_y = 0.1$ and $J_z = 1 - J_x - J_y$. Similarly, for gapped phase A_x (panel (c)), the parameters are $J_z = J_y = 0.1$ and $J_x = 1 - J_y - J_z$ and for gapped phase A_y (panel (d)), the parameters are $J_x = J_z = 0.1$ and $J_y = 1 - J_x - J_z$. Note that Dirac cone appears only for gapless phase B and vanish into Brillouin zone as the coupling is made anisotropic leading to gapped phases A_x , A_y , A_z .

II. DETECTING QUANTUM NOISE USING TDNEGF

Given a time-dependent Hamiltonian,

$$\mathbf{H}(t) = \sum_{ij} \mathbf{H}_{ij}(t) \hat{c}_i^\dagger \hat{c}_j \quad (3)$$

Here \hat{c}_i^\dagger , \hat{c}_i are single particle Fermionic creation (annihilation) operator on site i that includes spin and other orbital degree of freedom. The current operator for electrode μ is given by,

$$\hat{I}_\mu(t) = \sum_{ij\epsilon\mu} [\mathbf{H}_{ij}(t) \hat{c}_i^\dagger \hat{c}_j - \mathbf{H}_{ji}(t) \hat{c}_j^\dagger \hat{c}_i] \quad (4)$$

* bnikolic@udel.edu

Now, the current-current correlation function is defined as,

$$S_{\mu\nu}(t, t') = (\hat{I}_\mu(t) - \langle \hat{I}_\mu(t) \rangle) \times (\hat{I}_\nu(t') - \langle \hat{I}_\nu(t') \rangle) \quad (5)$$

Let us recall that lesser and retarded green functions are defined as,

$$G_{i,j}^r(t, t') = -i\Theta(t - t')\langle \{\hat{c}_i(t), \hat{c}_j^\dagger(t')\} \rangle \quad (6)$$

$$G_{i,j}^<(t, t') = i\langle \hat{c}_j^\dagger(t')\hat{c}_i(t) \rangle \quad (7)$$

A. Wave-function Approach

Keldysh green functions can be expressed in term wavefunction as follows,

$$G^r(t, t') = -i\Theta(t - t') \int \frac{dE}{2\pi} \sum_\alpha \Psi_{\alpha,E}(t)\Psi_{\alpha,E}^\dagger(t') \quad (8)$$

$$G^<(t, t') = i \sum_\alpha \int \frac{dE}{2\pi} f_\alpha(E) \Psi_{\alpha,E}(t)\Psi_{\alpha,E}^\dagger(t') \quad (9)$$

and

$$\begin{aligned} \langle \hat{c}_j^\dagger(t')\hat{c}_i(t) \rangle &= \frac{G_{ij}^<(t, t')}{i} \\ &= \sum_\alpha \int \frac{dE}{2\pi} f_\alpha(E) \Psi_{\alpha,E}^*(j, t')\Psi_{\alpha,E}(i, t) \end{aligned} \quad (10)$$

$$\langle \hat{c}_i(t)\hat{c}_j^\dagger(t') \rangle = \sum_\alpha \int \frac{dE}{2\pi} (1 - f_\alpha(E)) \Psi_{\alpha,E}(i, t)\Psi_{\alpha,E}^*(j, t') \quad (11)$$

Now, using Eq. 10, Eq. 11 in Eq. 5, one gets

$$\begin{aligned} S_{\mu\nu}(t, t') &= \sum_{\alpha, \beta} \int \frac{dE}{2\pi} \int \frac{dE'}{2\pi} f_\alpha(E)(1 - f_\beta(E')) \\ &\quad \times I_{\mu,EE'}(t)[I_{\nu,EE'}(t')]^* \end{aligned} \quad (12)$$

where,

$$\begin{aligned} I_{\mu,EE'}(t) &= \sum_{\langle ij \rangle \epsilon \mu} [\Psi_{\beta E'}^*(i, t)\mathbf{H}_{ij}(t)\Psi_{\alpha E}(j, t) \\ &\quad - \Psi_{\beta E'}^*(j, t)\mathbf{H}_{ji}(t)\Psi_{\alpha E}(i, t)] \end{aligned} \quad (13)$$

Signature of quantum noise can be found by plotting number of particles transmitted for a finite time interval Δ through a given electrode i.e. $\langle \hat{n}_\mu \rangle$ and its variance which are given by,

$$\langle \hat{n}_\mu \rangle = \sum_\alpha \int \frac{dE}{2\pi} f_\alpha(E) N_{EE} \quad (14)$$

$$var(\hat{n}_\mu) = \sum_\alpha \int \frac{dE}{2\pi} \int \frac{dE'}{2\pi} f_\alpha(E)(1 - f_\beta(E')) \times |N_{EE'}|^2 \quad (15)$$

$$N_{EE'} = \int_{\Delta/2}^{\Delta/2} I_{\mu,EE'}(t) \quad (16)$$

The formula for variance Eq. 15 is true for finite time Δ but a correction term needs to be added to capture $\Delta \rightarrow \infty$. Therefore, for $\Delta \rightarrow \infty$,

$$var(\hat{n}_\mu) = \sigma_{st}^2 \Delta + 2\sigma_{mix} + \bar{\sigma}^2 + O(\frac{1}{\Delta}) \quad (17)$$

Here first term corresponds to noise coming from stationary states and last two terms correspond to any added perturbation. The terms are given by,

$$\sigma_{st}^2 = \sigma_{\alpha, \beta} \int \frac{dE}{2\pi} f_\alpha(E)(1 - f_\beta(E))|I_{\mu,EE}(0)|^2 \quad (18a)$$

$$\sigma_{mix} = \sum_{\alpha, \beta} \int \frac{dE}{2\pi} f_\alpha(E)(1 - f_\beta(E))\mathcal{R}[\bar{N}_{EE}^* I_{\mu,EE}(0)] \quad (18b)$$

$$\bar{\sigma}^2 = \sum_{\alpha, \beta} \int \frac{dE}{2\pi} \int \frac{dE'}{2\pi} f_\alpha(E)[1 - f_\beta(E')]|\bar{N}_{EE'}|^2 \quad (18c)$$

with

$$\bar{N}_{EE'} = \int_{-\infty}^{\infty} dt [I_{\mu,EE'}(t) - I_{\mu,EE'}(0)e^{-i(E-E')t}]$$

Note the first term in Eq. 17 is diverges as $\Delta \rightarrow \infty$. One can always subtract that contribution from total to get noise contribution from perturbative part.

III. KITAEV SPIN LIQUID

We know that specific heat for quantum case has two peaks as temperature is increased. We also know that C_v increases as T decreases for classical spin liquid. We used monte carlo simulation to compute C_v for classical spin liquid for our device.

$$C_v = \frac{\langle E^2 \rangle - \langle E \rangle^2}{k_B T^2} \quad (19)$$

where $\langle E^2 \rangle$ and $\langle E \rangle$ were obtained using monte carlo at a given temperature T for classical case. For quantum case, we assumed all spins as spin $\frac{1}{2}$ particles and compared result of TPQ states with exact result and obtained $\langle E^2 \rangle$ and $\langle E \rangle$ as follows :

For ED :

$$\langle E^2 \rangle = \text{Tr}[\hat{\rho}\hat{H}^2] \quad (20)$$

$$\langle E \rangle = \text{Tr}[\hat{\rho}\hat{H}] \quad (21)$$

$$\hat{\rho} = \frac{e^{-\beta \hat{H}}}{Z} \quad (22)$$

$$Z = \text{Tr}[e^{-\beta \hat{H}}] \quad (23)$$

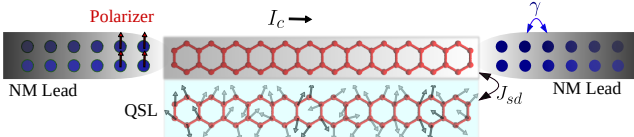


FIG. 3. Device description

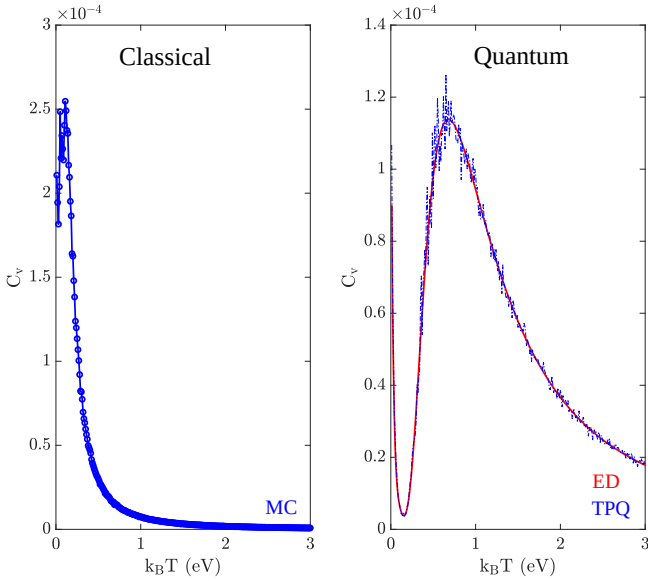


FIG. 4. The figure above shows comparison of heat capacity as function of temperature for classical versus quantum case. Heat capacity for classical case was computed using monte carlo simulation. The quantum case was computed using exact diagonalization and using TPQ. One may note that TPQ traces exact result closely with some noise. The important thing to note here is that classical case shows increased C_v as $k_B T$ decreases whereas quantum case shows two such peaks : one close to zero and another one around $0.7 k_B T$. The low temperature peak for quantum case is not prominent. It is not clear whether it is due to missing periodic boundary condition.

A. Time evolution

The spin correlation for each site is calculated in quantum case using :

$$\langle \hat{S}_i^\alpha(0) \hat{S}_i^\alpha(t) \rangle = \text{Tr} [\hat{\rho} \hat{S}_i^\alpha(0) e^{\frac{i\hat{H}t}{\hbar}} \hat{S}_i^\alpha(0) e^{-\frac{i\hat{H}t}{\hbar}}] \quad (24)$$

$$\langle \hat{S}_i^\alpha(t) \rangle = \text{Tr} [\hat{\rho} e^{\frac{i\hat{H}t}{\hbar}} \hat{S}_i^\alpha(0) e^{-\frac{i\hat{H}t}{\hbar}}] \quad (25)$$

Here α represent x, y, z components of spin operators \hat{S}_i^α at site i . For TPQ states :

$$\langle \hat{A} \rangle_{\text{TPQ}} = \langle \Psi_{\text{TPQ}} | \hat{A} | \Psi_{\text{TPQ}} \rangle \quad (26)$$

$$| \Psi_{\text{TPQ}} \rangle = e^{\frac{-\beta \hat{H}}{2}} | \Psi_0 \rangle \quad (27)$$

$$| \Psi_0 \rangle = \sum_i c_i | i \rangle \quad (28)$$

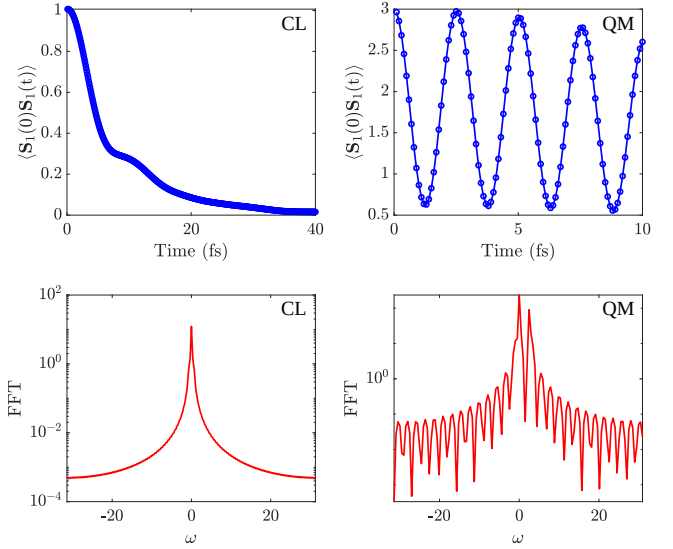


FIG. 5. The figure above shows average onsite spin correlation and a comparison between classical versus quantum case. One may note that for classical case, the onsite autocorrelation decays exponentially with time as expected. But for quantum case, we see decay but with stringer precessional motion. Performing FFT on both classical and quantum onsite correlations reveal difference in peaks in frequency domain. Here, to capture ground state dynamics of Kitaev Hamiltonian, we stayed close to ground state with $\langle E \rangle = -2.475$ eV with $E_{\min} = -2.496$ eV

Here $\sum_i |c_i|^2 = 1$ Note the classical spins were evolved using classical Heisenberg equation of motion :

$$\frac{d\hat{S}_i^\alpha}{dt} = i [\hat{H}, \hat{S}_i^\alpha] \quad (29)$$

N number of independent initial spin configurations \hat{S}_i^α are obtained from monte carlo simulation and evolved in time according to the equation above independently. Average onsite spin correlation is therefore obtained by averaging over these configurations and sites as mentioned in Eq. 6 of [2] :

$$\langle \hat{\mathbf{S}}(0) \hat{\mathbf{S}}(t) \rangle = \langle \hat{\mathbf{S}}(0) \hat{\mathbf{S}}(t) \rangle_{\text{config,site}} \quad (30)$$

B. Adding electron using TD2D

Now let us see how this spin dynamics affects the electron when coupled using $s-d$ interaction.

$$\hat{H}_{sd} = -J_{sd} \sum_i \text{Tr} [\hat{\rho} |i\rangle \langle i| \otimes \hat{\sigma}] \cdot \hat{\mathbf{S}}_i \quad (31)$$

what happens when z-spin polarized current is injected in Az (done), Ax (in progress), Ay and gapless phases

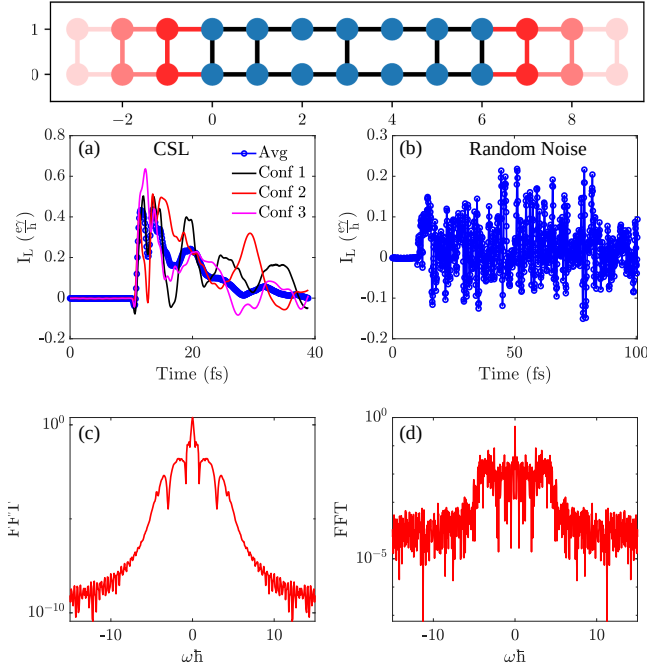


FIG. 6. The figure above shows charge current driven by classical spin liquid (panel (a), (c)) and a comparison of noise driven charge current. Classical spin liquid correlation is measured by averaging over several spin configurations. Here, 15 such configurations have been used to check how charge current will be driven when coupled through J_{sd} . The average charge current over those configurations is shown as well. Panel (c) shows FFT of configuration averaged charge current which shows total 5 peaks. Panel (b) shows charge current driven by random noise and panel (d) shows the FFT of that. The device structure is shown on top.

- [1] J. Knolle, D. Kovrizhin, J. Chalker, and R. Moessner, “Dynamics of a two-dimensional quantum spin liquid: signatures of emergent majorana fermions and fluxes,” *Physical Review Letters*, vol. 112, no. 20, p. 207203, 2014.

- [2] M. Taillefumier, J. Robert, C. L. Henley, R. Moessner, and B. Canals, “Semiclassical spin dynamics of the anti-ferromagnetic heisenberg model on the kagome lattice,” *Physical Review B*, vol. 90, no. 6, p. 064419, 2014.

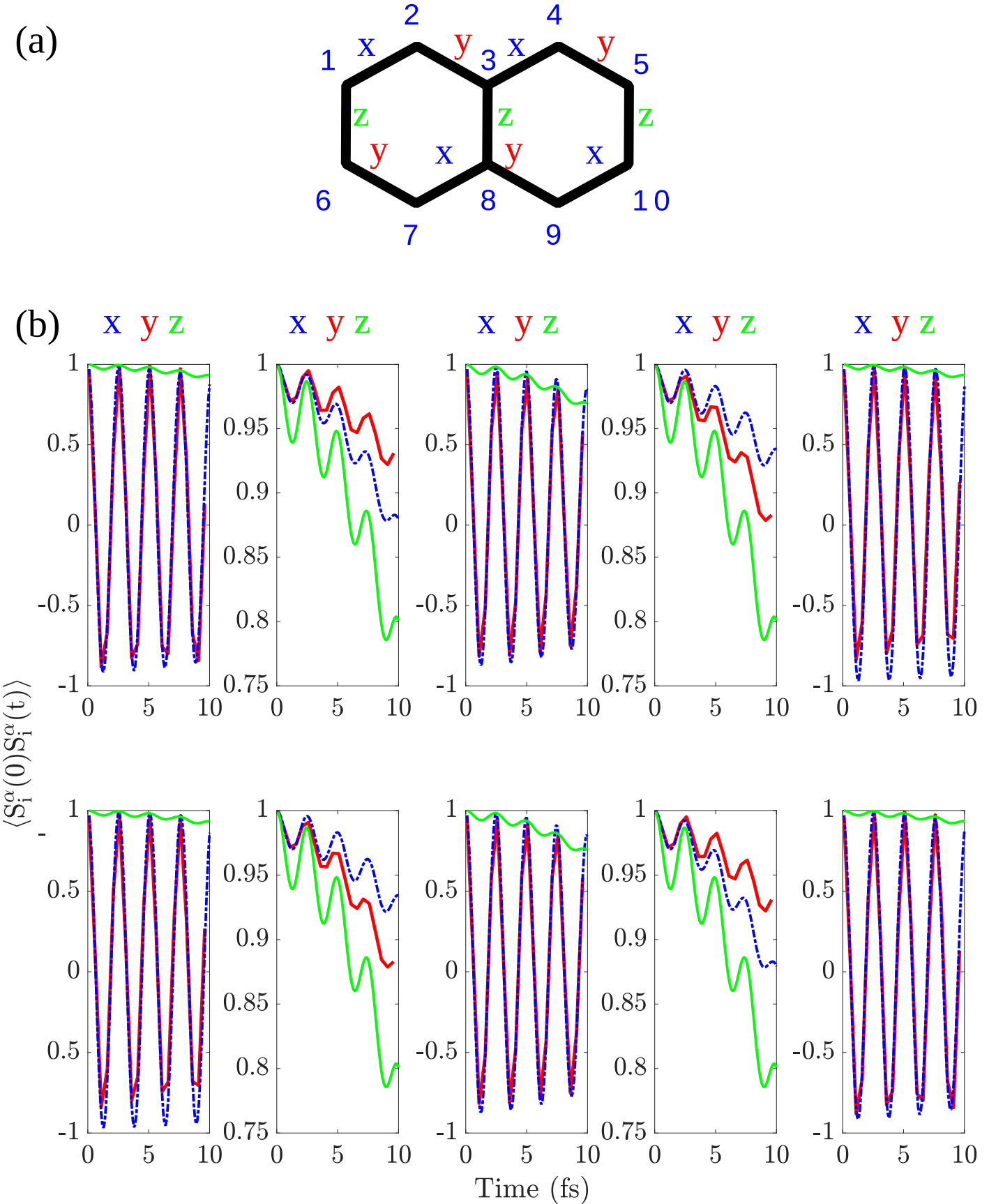


FIG. 7. The figures above shows spin dynamics of individual spin of device structure shown above. The parameters chosen are $K_x = K_y = 0.1$ and $K_z = 1 - K_x - K_y$ i.e. A_z phase. The top panels show spin dynamics of first layer i.e. site 1 through 5 and bottom panel shows individual spin dynamics for bottom layer i.e. site 6 to 10. From symmetry of device structure, we expect spins at site 1, 3, 5, 6, 8, 10 to have similar dynamics and indeed we see that is indeed the case. Also, by comparing the symmetry of site 2 and 7 we see that their x and y bonds are switched in device structure and as a result the spin dynamics is also switched (shown in panel). We do see spins precessing but the same time decaying with time as well. This calculation is done using ED.

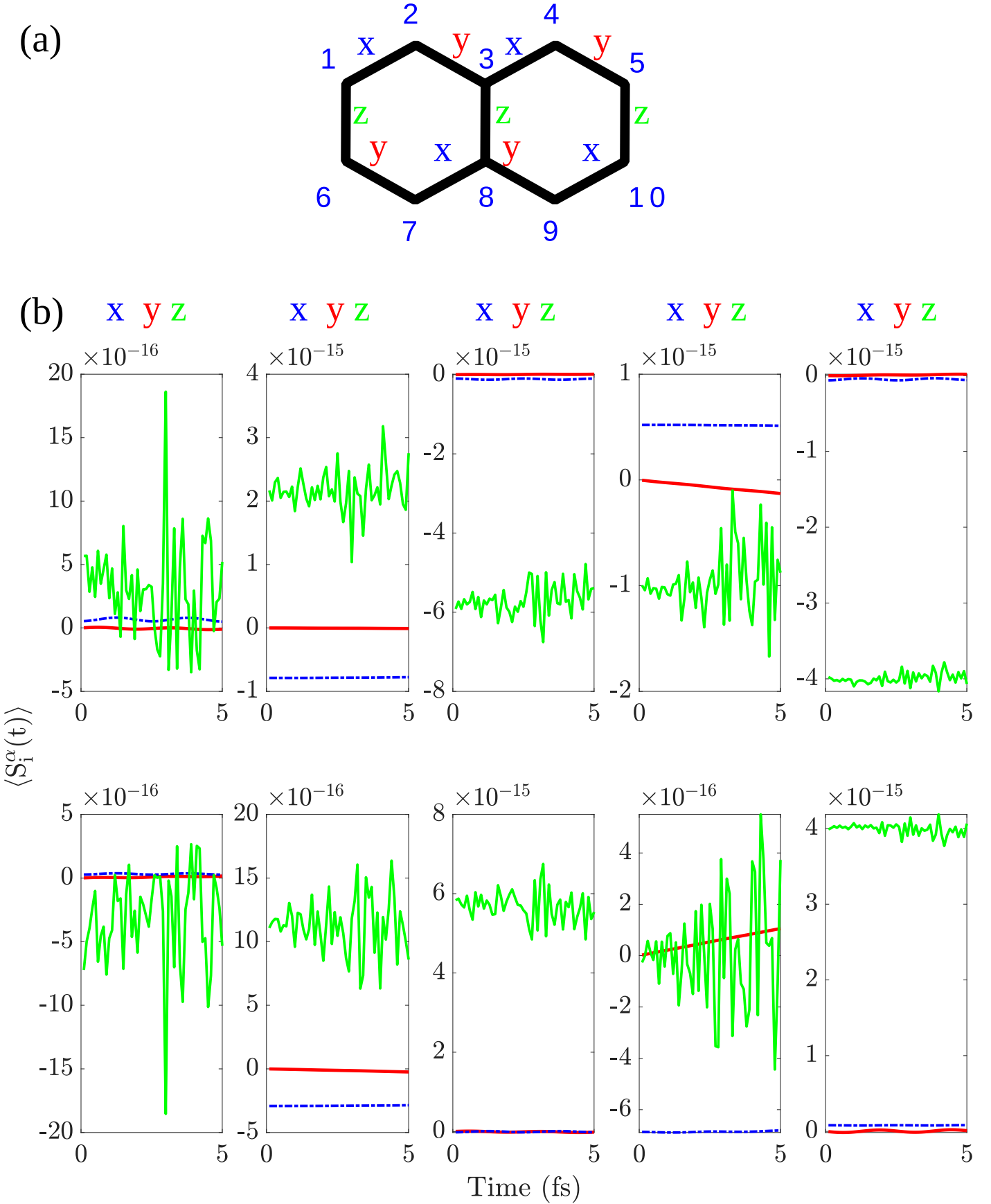


FIG. 8. Since the ground state of Kitaev Hamiltonian, although the spins have non-zero onsite correlation, all spin expectation value for each spin is zero. Panel (a) shows device structure same as before and panel (b) shows spin density at each site. The top five panels of panel (b) show spin density for layer one of device shown in panel (a) i.e. site, 1, 2, 3, 4, 5. Similarly, bottom panels show spin density for bottom layer i.e. site 6, 7, 8, 9, 10. It can be seen that all spin expectation value i.e. $S_i^\alpha = 0$ where i is site index and α is x, y, z component respectively.

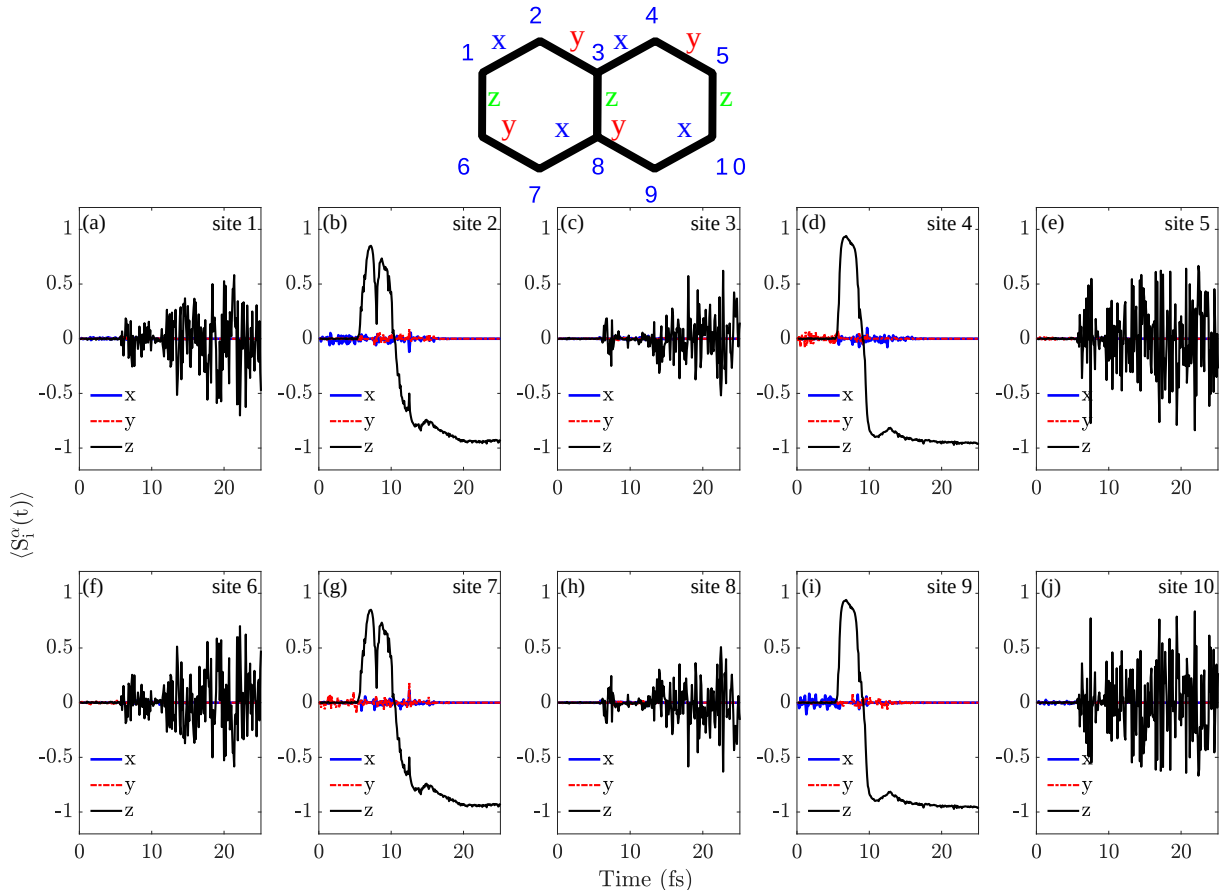


FIG. 9. Dynamics of local spins initially kept at A_z quantum spin liquid phase and excited by z-spin polarized electron. Here $J_z \gg J_x, J_y$, $T = 30$ K

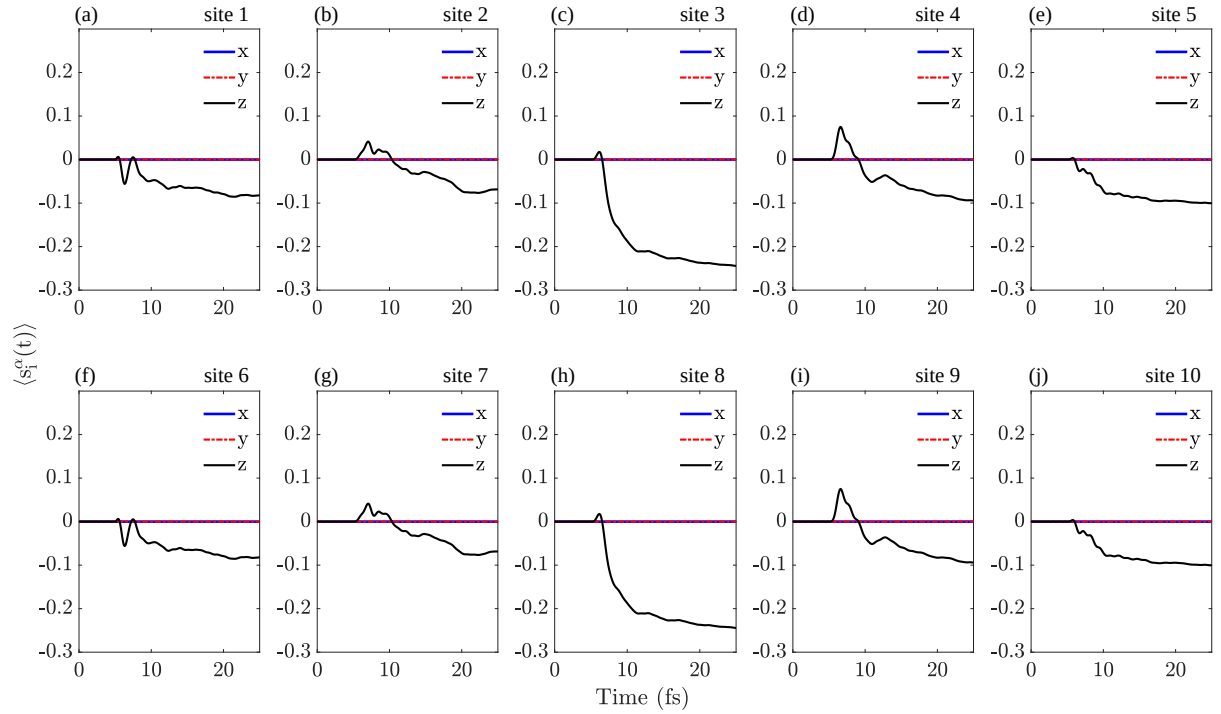


FIG. 10. electron spin density at site 1 from td2d.

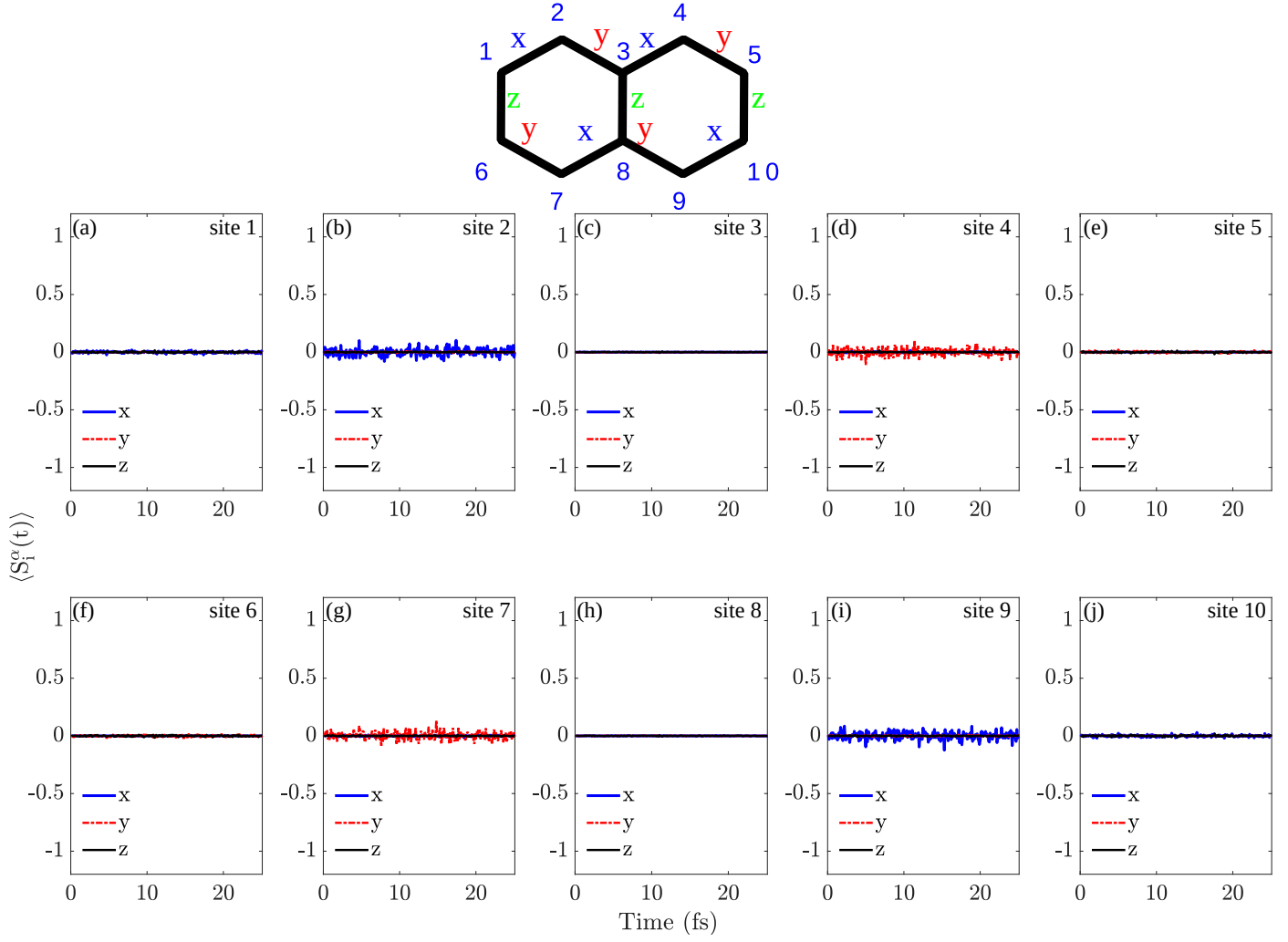


FIG. 11. Dynamics of local spins initially kept at A_z quantum spin liquid phase i.e. $J_z \gg J_x, J_y$, Temperature $\mathbf{T} = 30$ K, $\mathbf{J}_{sd} = 0$ eV

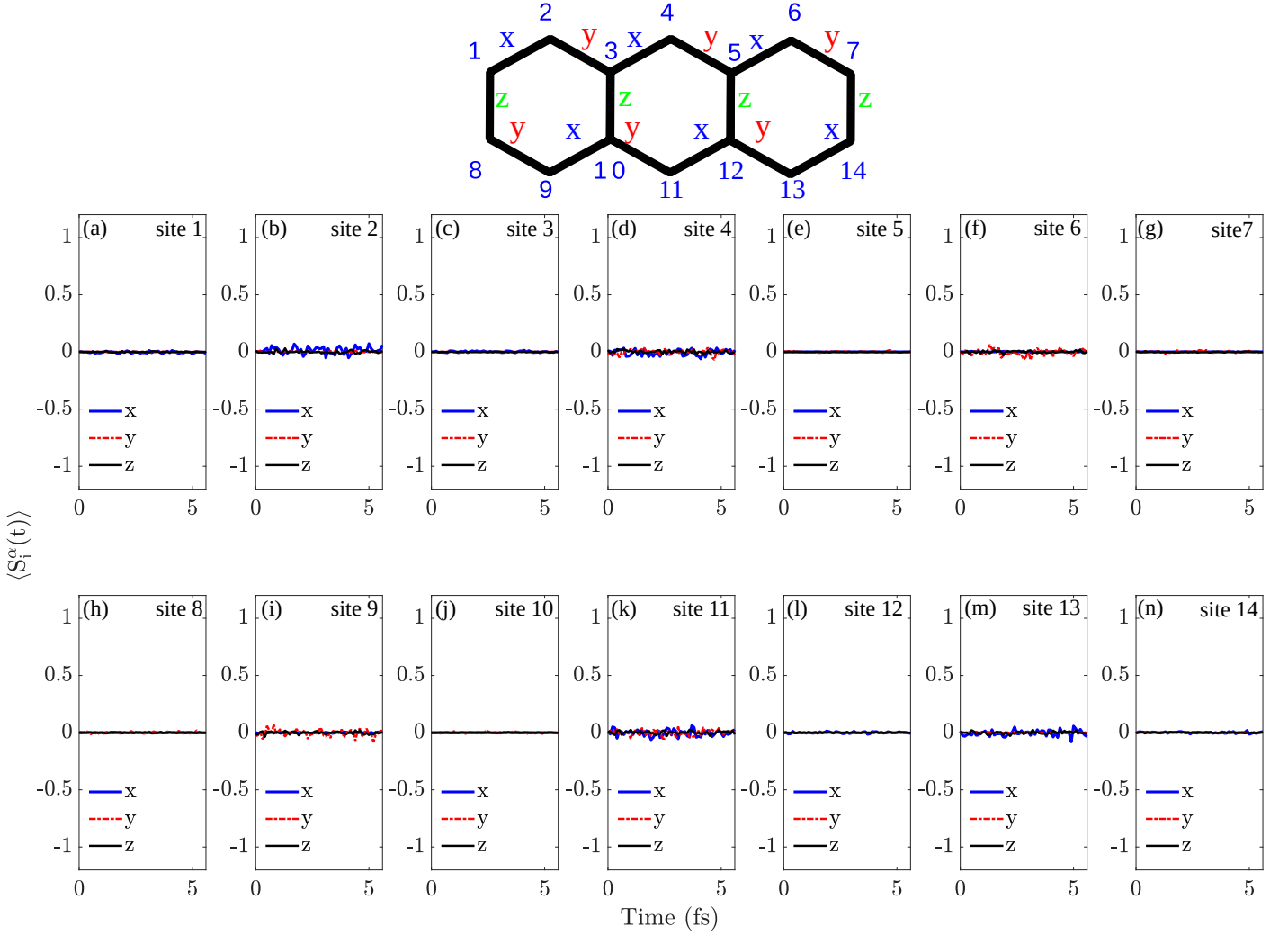


FIG. 12. Dynamics of local spins initially kept at A_z quantum spin liquid phase i.e. $J_z \gg J_x, J_y$ for slightly bigger system size, Temperature $T = 30 K$, $\mathbf{J}_{sd} = 0$ eV, Larger system size : 7×2

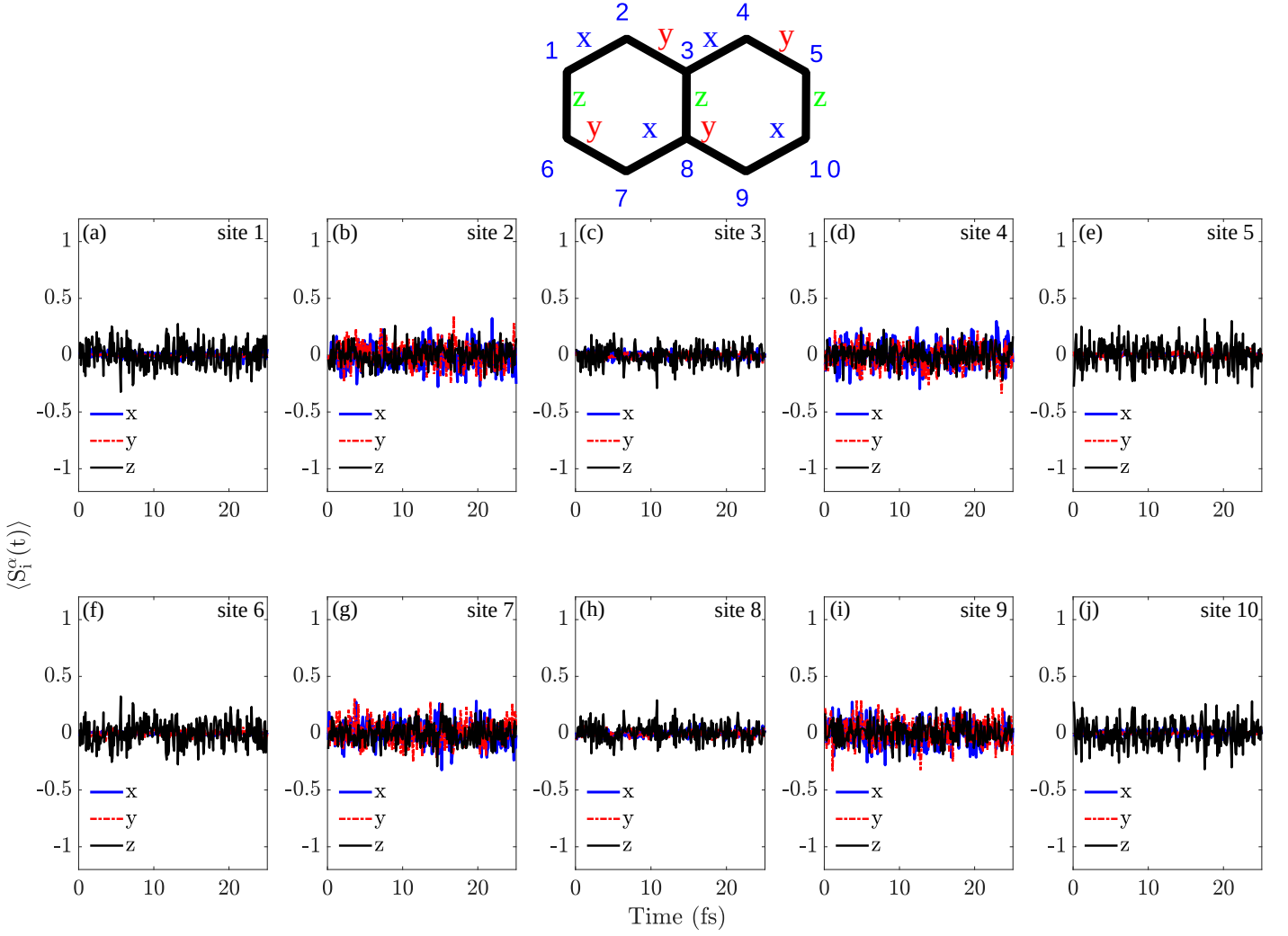


FIG. 13. Dynamics of local spins initially kept at A_z quantum spin liquid phase i.e. $J_z \gg J_x, J_y$ when temperature is increased 10 times, **Temperature T = 300 K, $J_{sd} = 0$ eV**

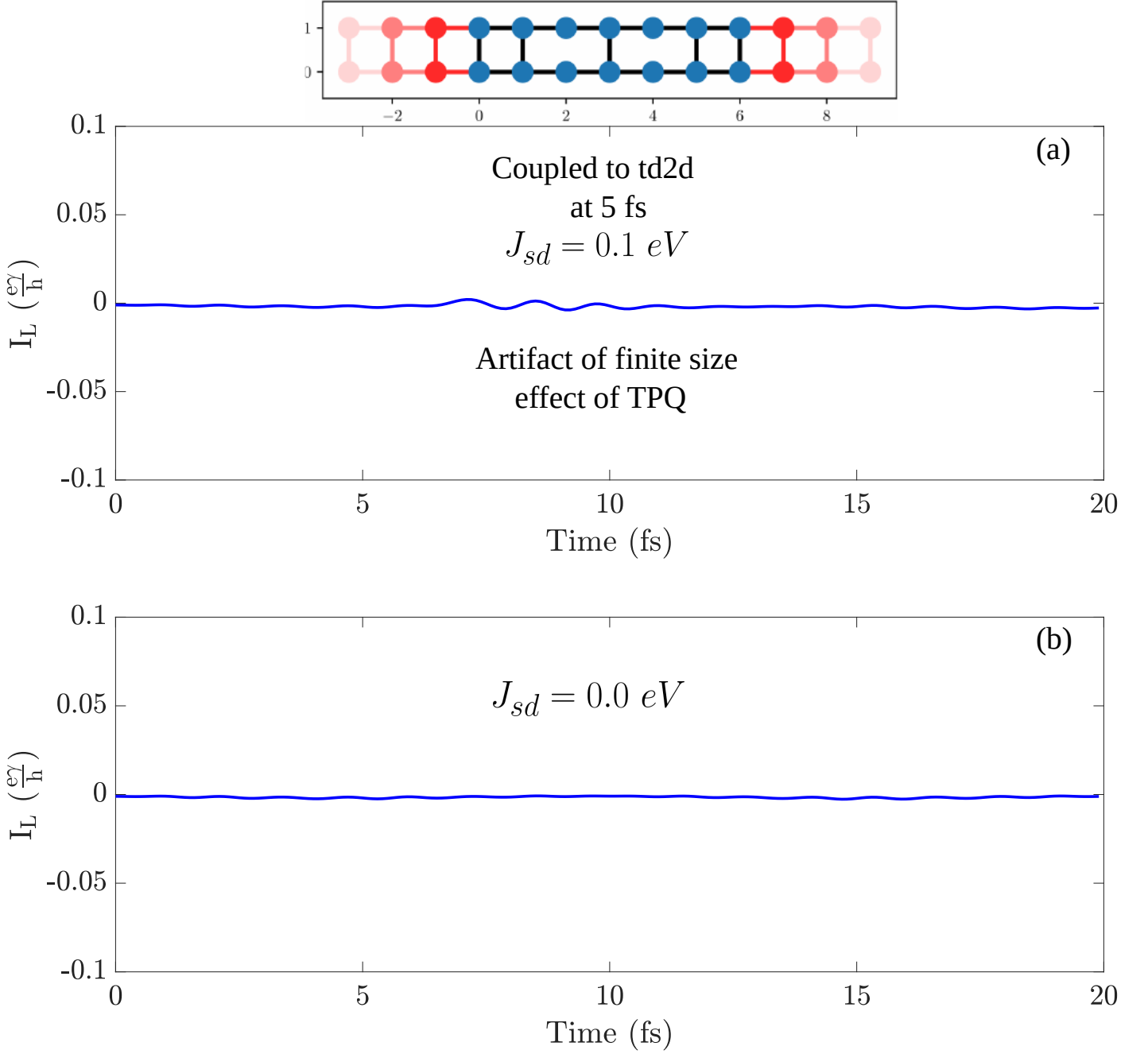


FIG. 14. When local spin density computed using TPQ is coupled to TD2D we see some artifact charge current generated for $J_{sd} \neq 0$. Such current are absent when $J_{sd} = 0$. Here temperature, $T = 30 K$

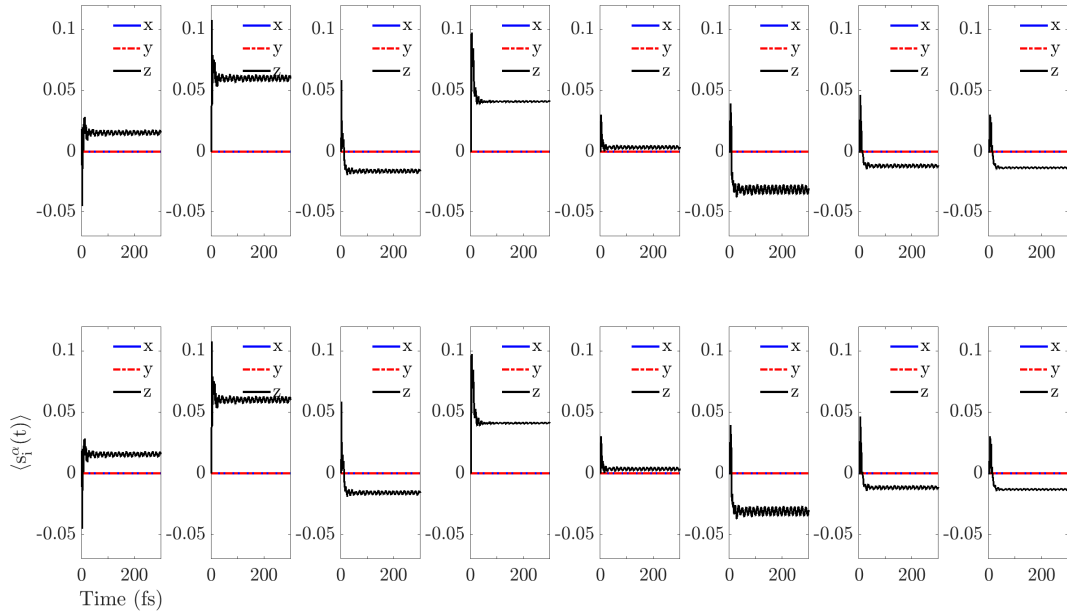


FIG. 15. Caption : warm up 300 fs

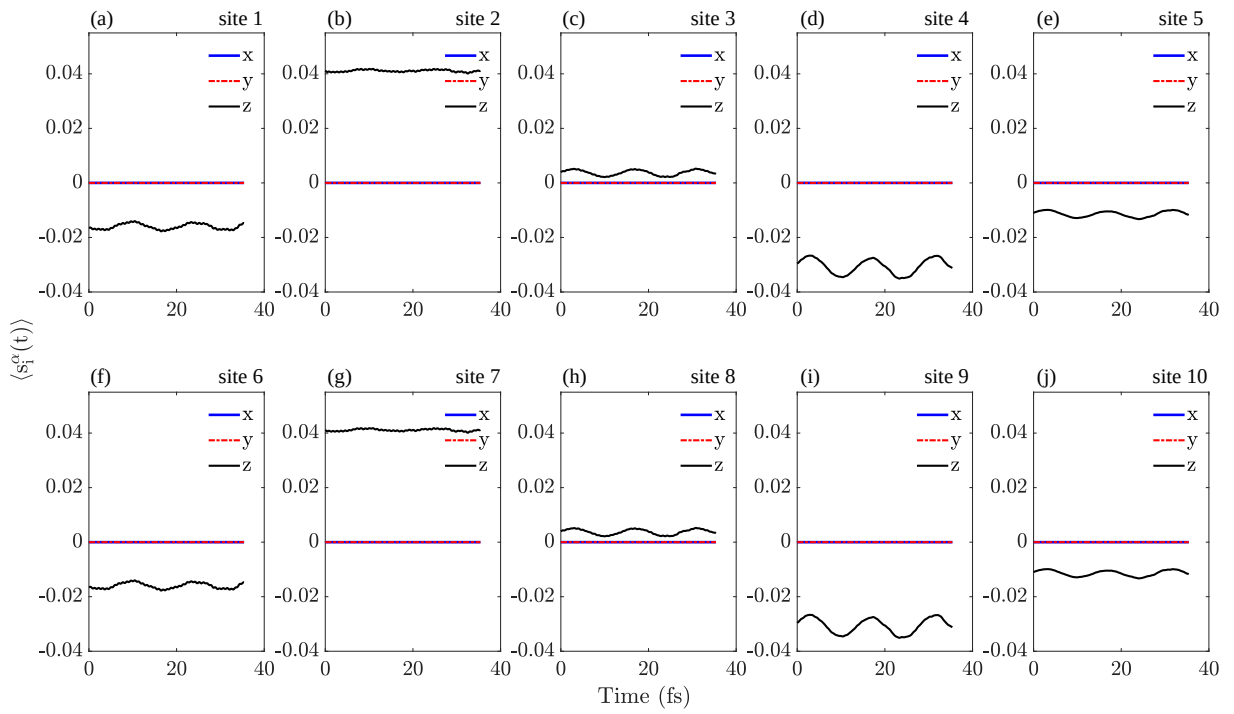


FIG. 16. Caption

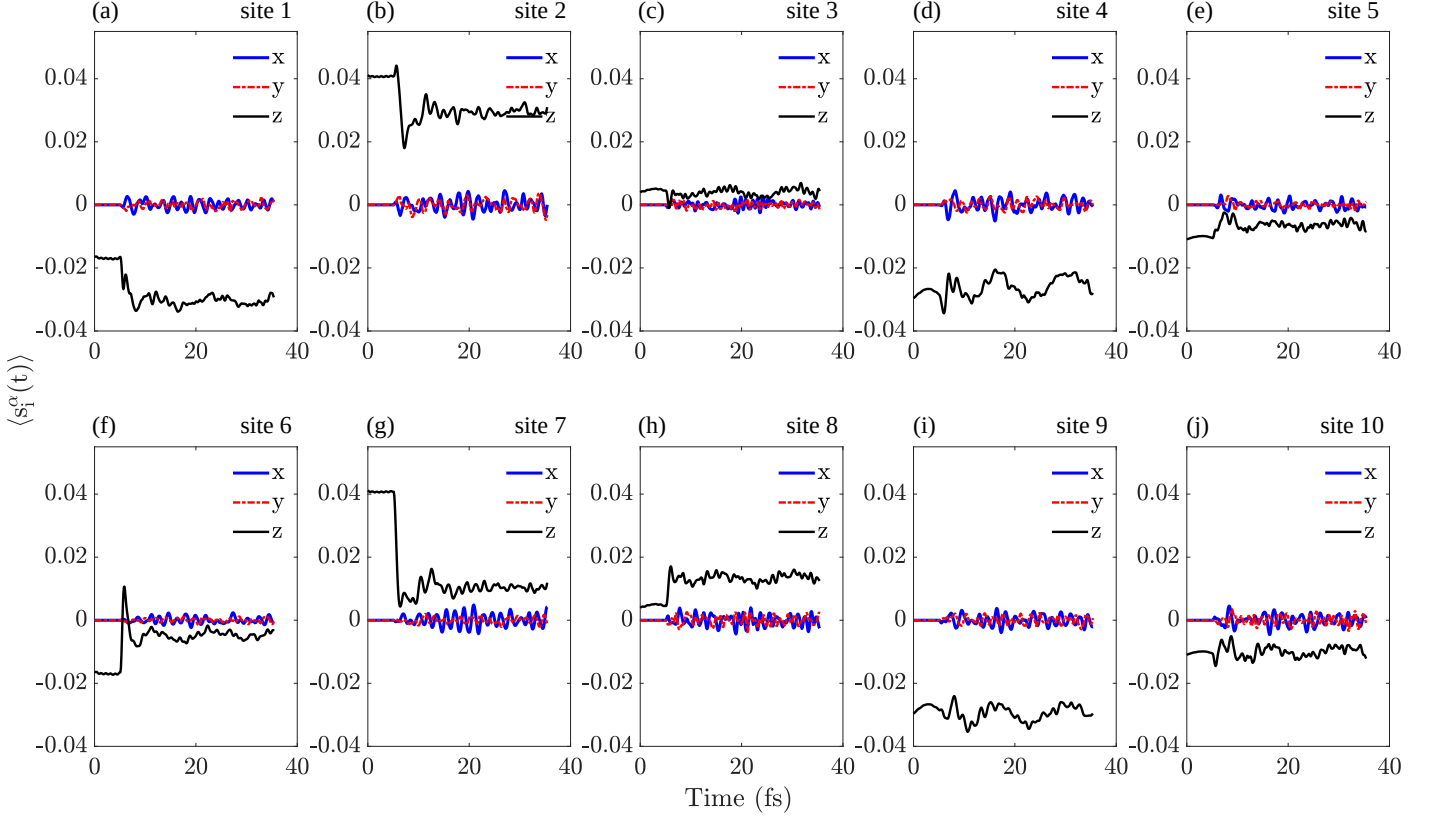


FIG. 17. Do this plot for test case to check direction of local spin polarization. Here Do this plot for test case to check direction of local spin polarization. Do this plot for test case to check direction of local spin polarization. Do this plot for test case to check direction of local spin polarization. Here Do this plot for test case to check direction of local spin polarization. Do this plot for test case to check direction of local spin polarization.

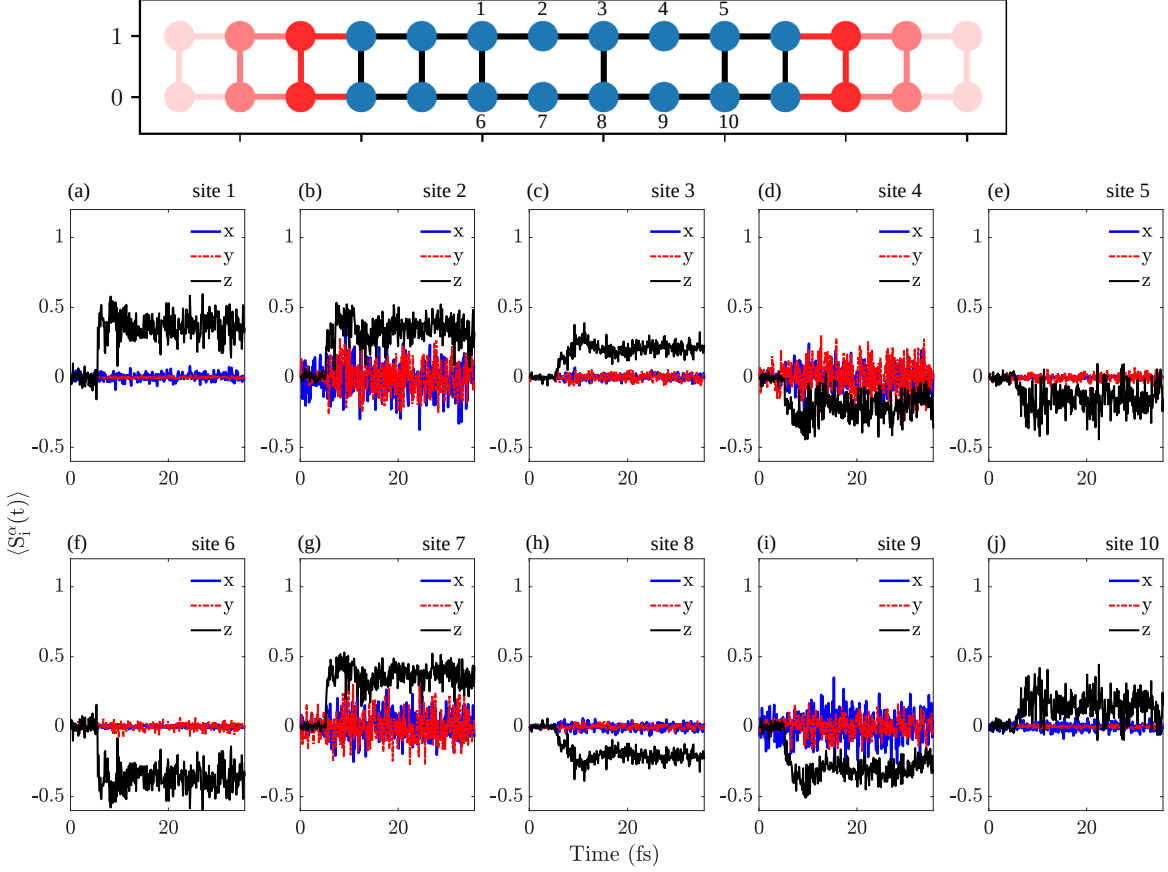


FIG. 18. The local spin dynamics when z-spin polarized current is injected into the QSL A_z phase at $T = 50$ K. $J_{sd} = 0.1$ eV. Applied bias is 0.05 eV

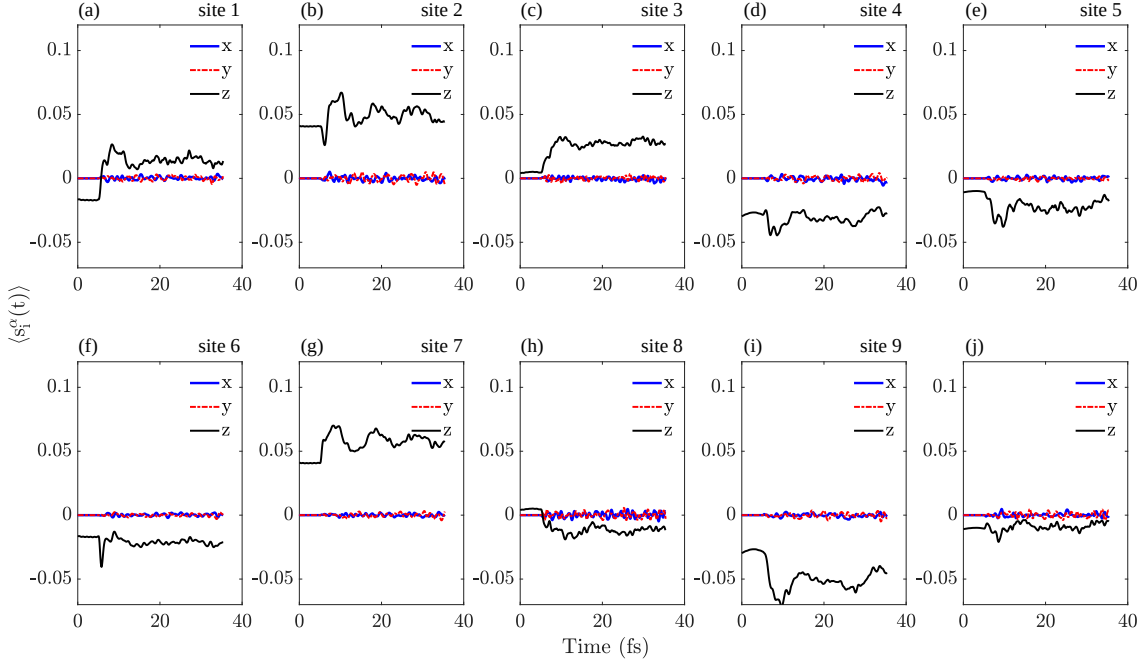


FIG. 19. Electron spin density dynamics due to feedback switched on at $t = 5$ fs

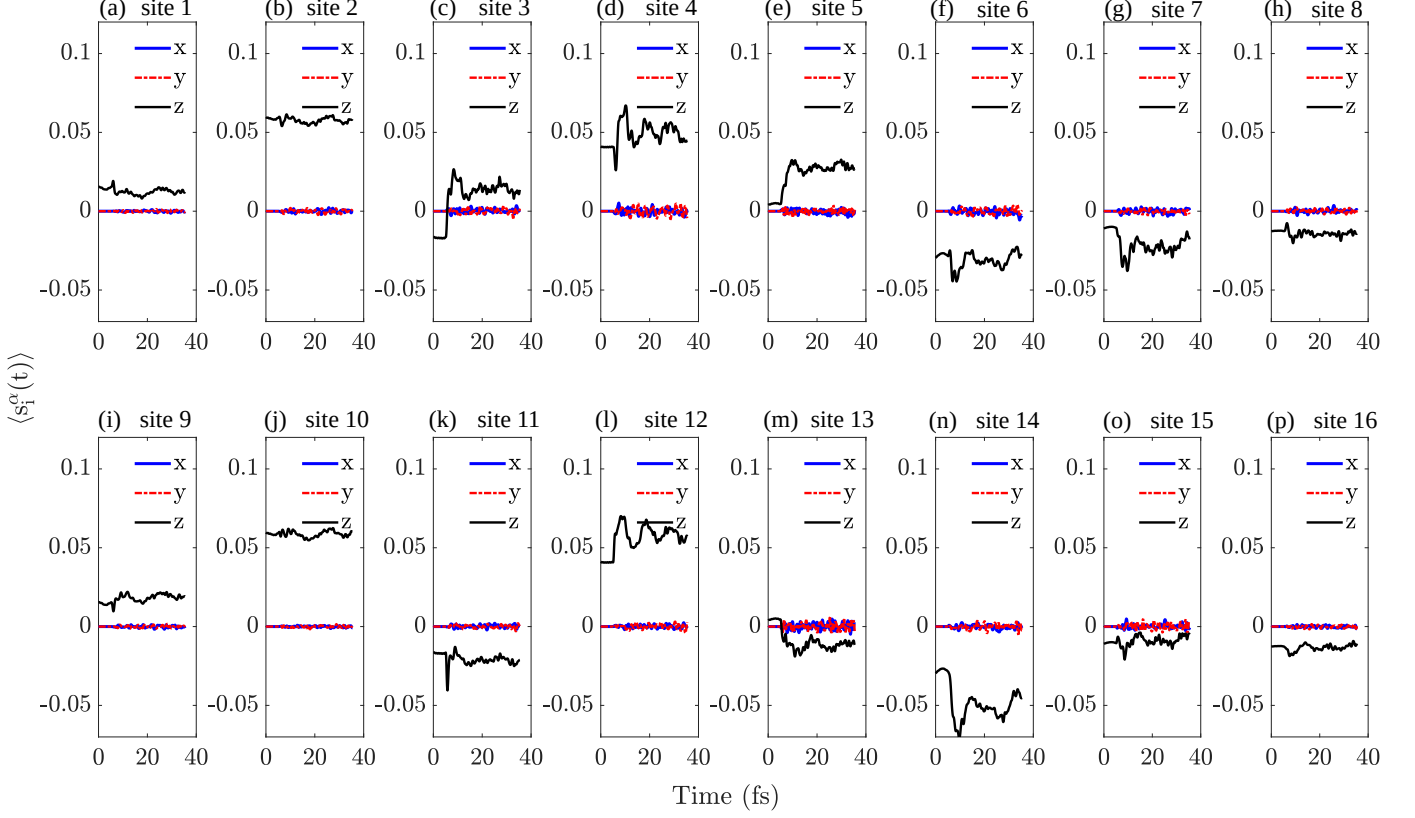
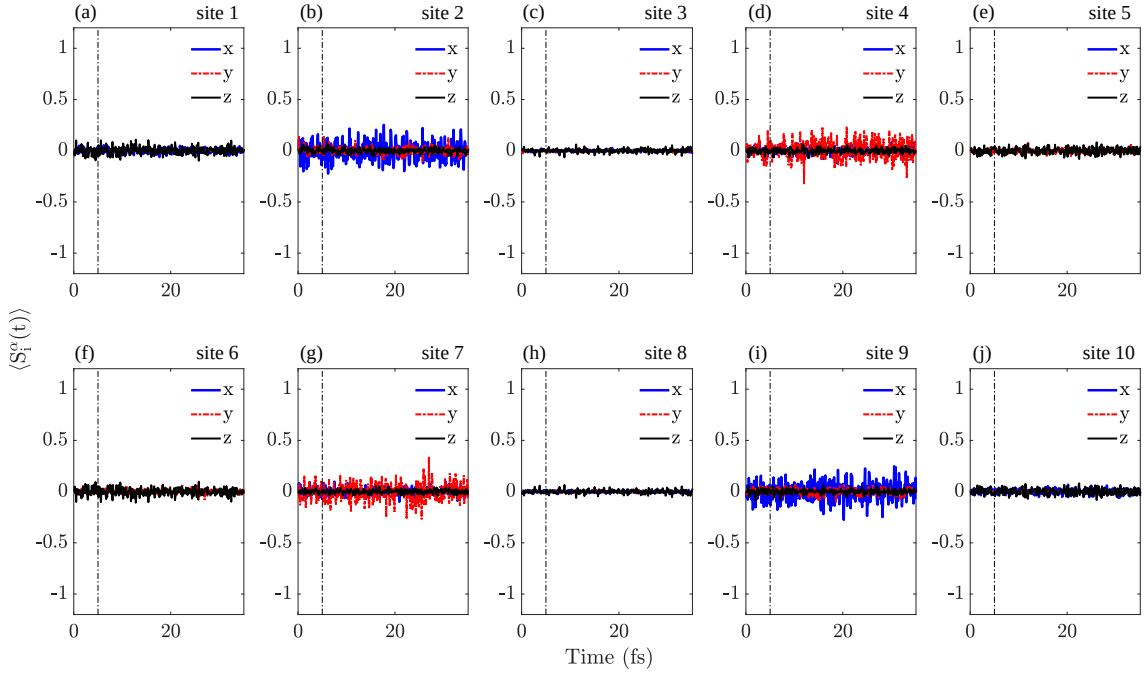
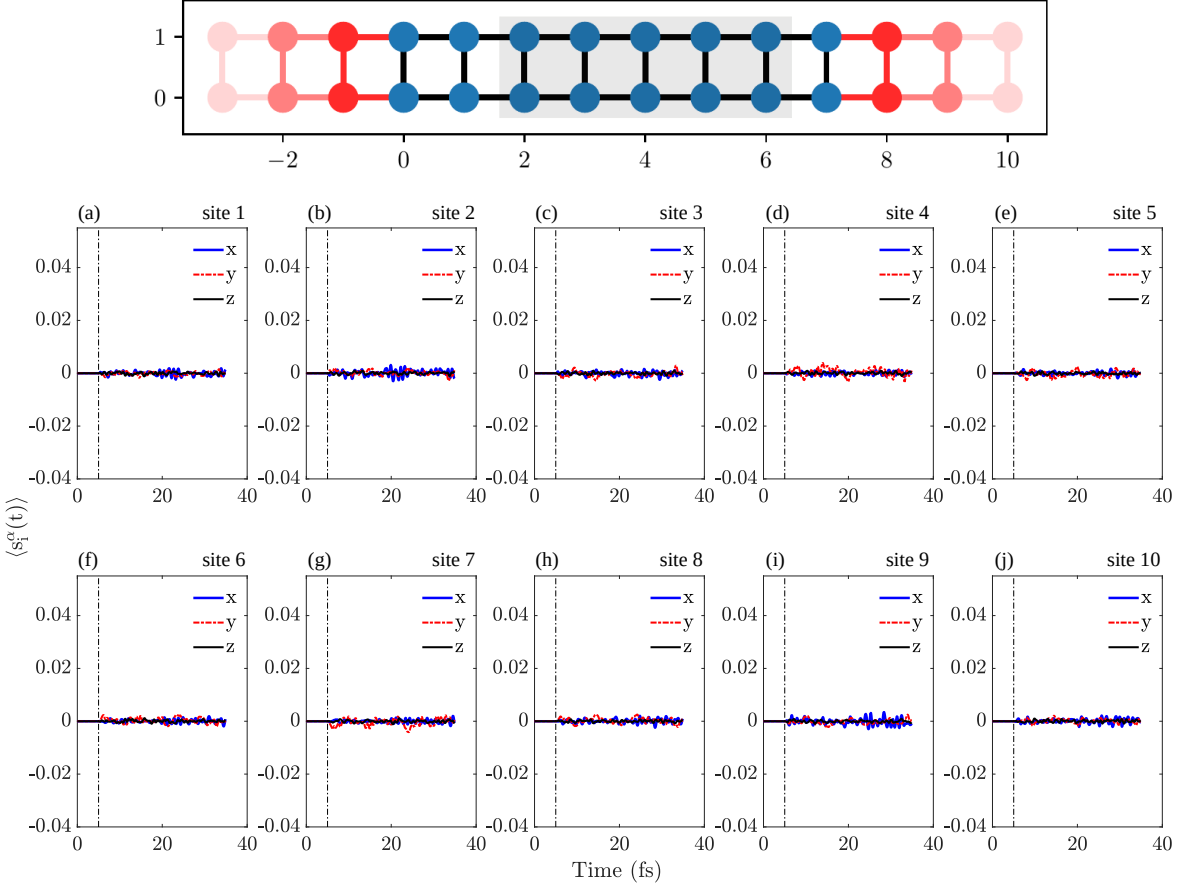


FIG. 20. Local electron spin density with lead sites. Note left lead includes $2 \times 2 = 4$ polarizers.



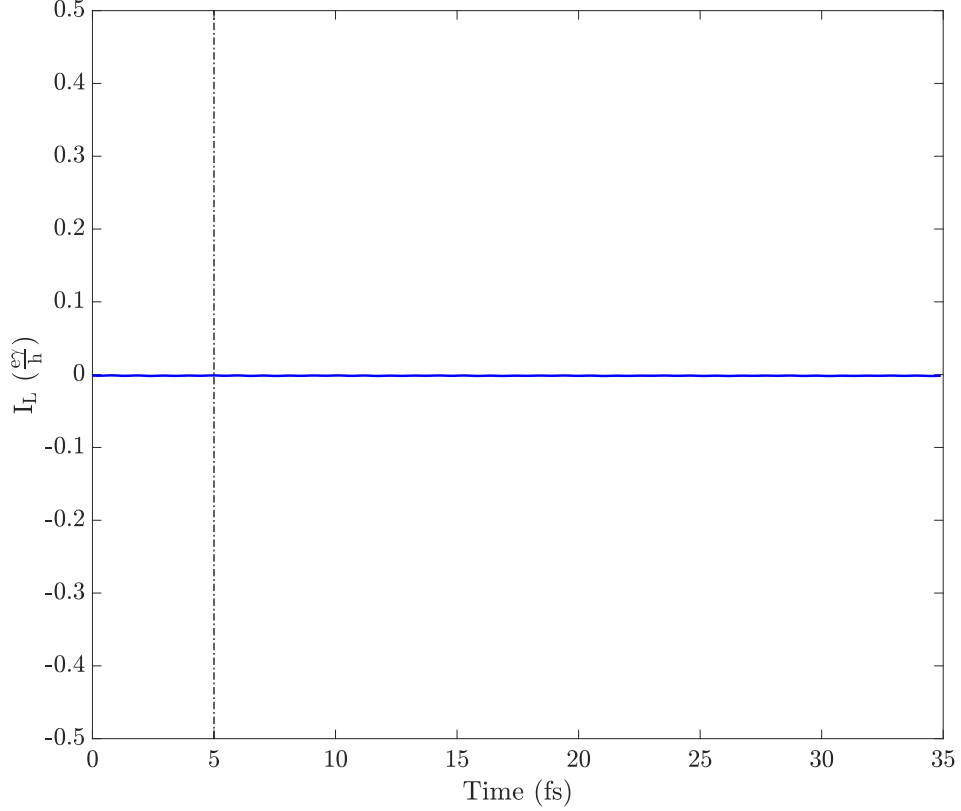


FIG. 23. Charge current with no bias and no injected spin current. In the absence of any electron spin polarization, there is no detectable charge current even after the feedback coupling is switched on after $t = 5 \text{ fs}$.

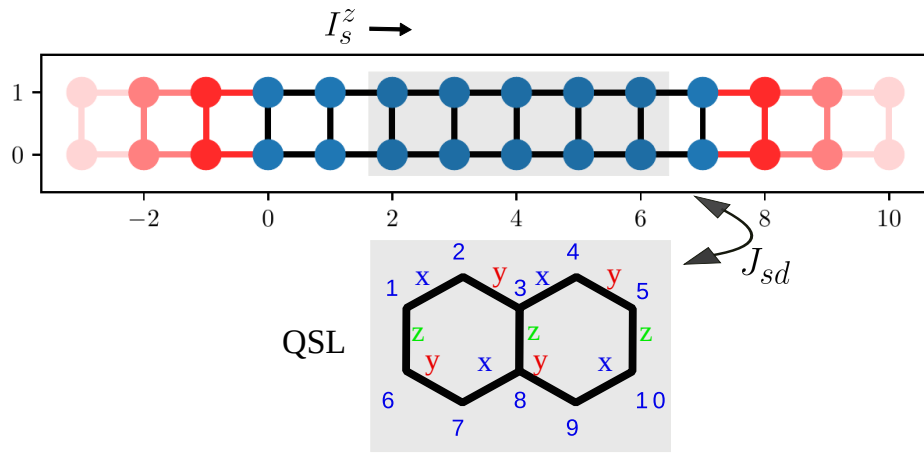


FIG. 24. Device description : z- spin polarized current is injected into ladder which interacts with QSL in A_z phase via J_{sd} coupling. Since, we will consider feedback coupling, the QSL spin dynamics and local electron spin dynamics can affect each other. All results from this point onwards are for z- spin polarized current injected into ladder.

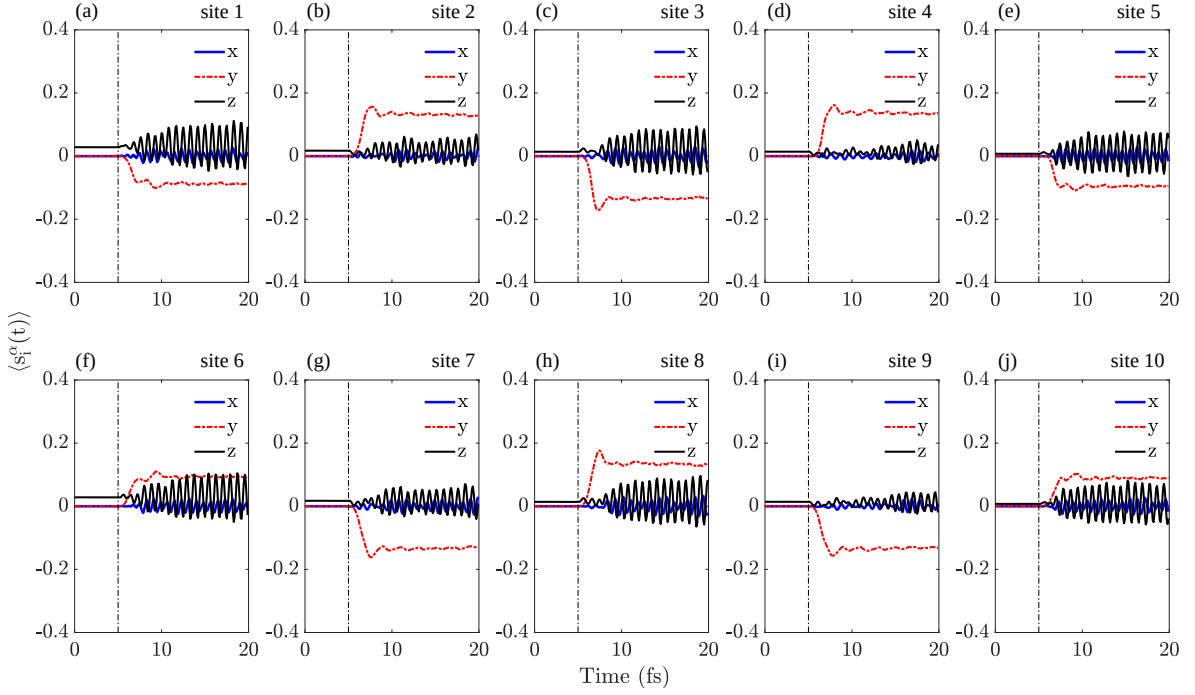


FIG. 25. The figure above shows local electron spin density dynamics when z-spin polarized current is injected into QSL in A_z phase with feedback. The coupling between electron and QSL is switched on at $t > 5$ fs. The local electron spin density was +z spin polarized (black) before $t < 5$ fs and as soon as the feedback coupling is switched on, we see precession of x-, z- component (blue, black) with net spin along y-direction(red). Injected z- spin polarized electron was converted to y-spin polarized electron as the coupling between TDNEGF and QSL is switched on with feedback. Here, $J_{sd} = -0.3$ eV and applied bias = 0.05 eV, Temperature, $T = 50$ K.

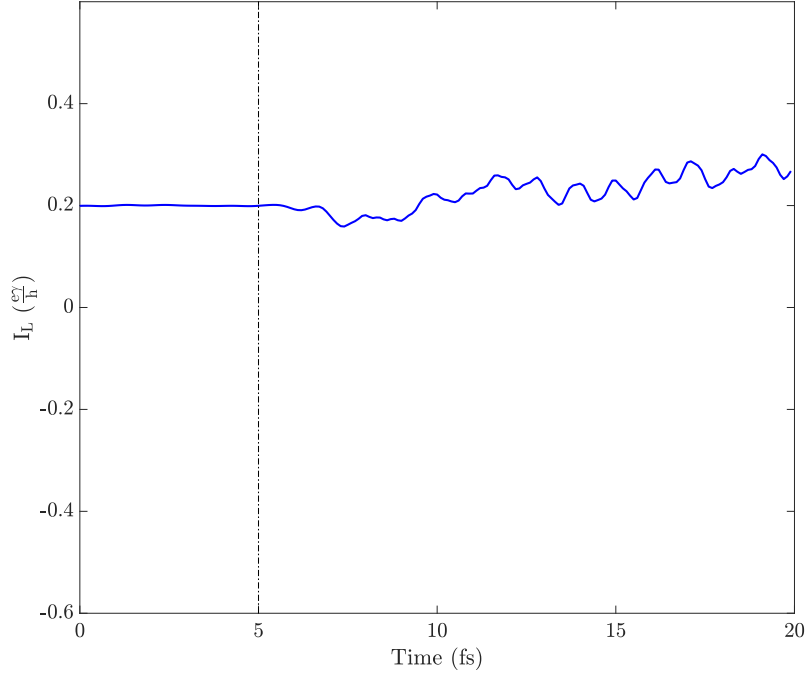


FIG. 26. The figure above shows charge current dynamics when feedback coupling between TDNEGF and QSL in A_z phase is switched on. Since, our metal device is a ladder, we see that current is conductance ($G = 4 \frac{e^2}{h}$ for ladder) times applied bias (0.05 eV here). Switching on feedback coupling after 5 fs (shown with dashed black line) captures noise driven charge current as a result of the coupling. Here, $J_{sd} = -0.3$ eV

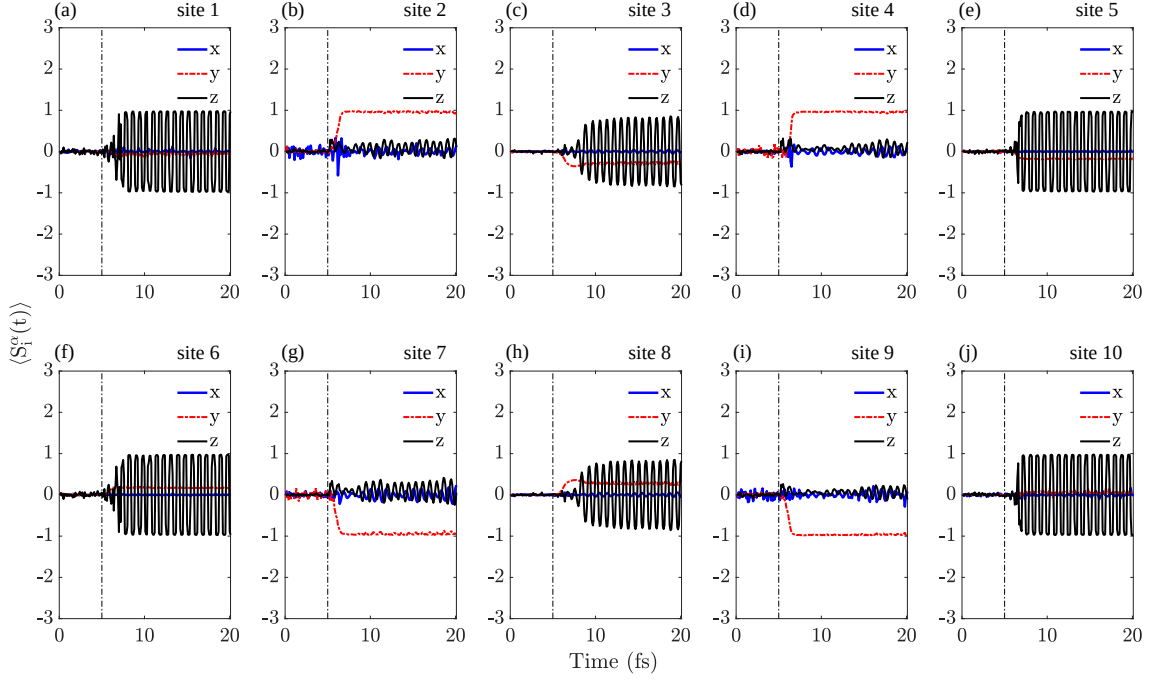


FIG. 27. The figure above shows the local spin dynamics in QSL as a result feedback coupling with electron switched on after $t = 5$ fs (shown with dashed black line). We see precession in z-component (black) in all 10 spins of QSL. The spin liquid in A_z phase means $J_z \gg J_x, J_y$ and therefore spins at site 2, 4, 7, 9 are loosely coupled (J_x, J_y) to nearest neighbour. When z-spin polarized current is injected into QSL with feedback, due to weak coupling, torque on these sites convert these spins to y-spin polarization. For the sites that are strongly coupled via J_z coupling, show precession in z-component but the net y-spin polarized component are small at these sites. It is possible that there is a competition between torque by injected z-spin polarized electron and that coming from J_z coupling of Kitaev spin liquid. Torque by injected z-spin polarized current dominates only at weakly coupled site converting to y-spin polarization. The spin dynamics is likely to vary for different QSL phase such as A_x , A_y or gapless QSL phase.

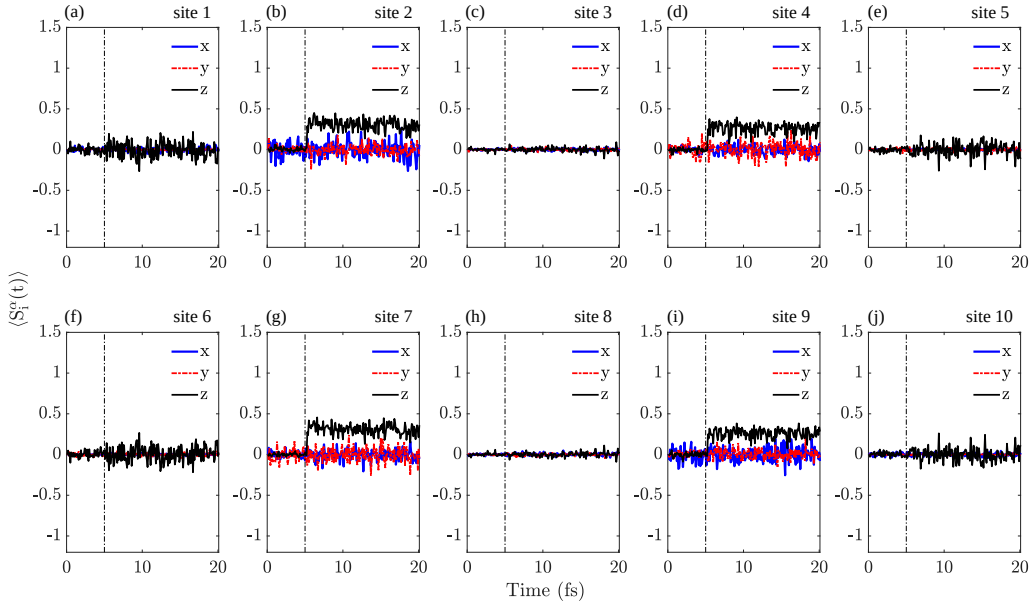


FIG. 28. If the feedback is switched off i.e. spin polarized electrons are injected into QSL but no feedback from QSL to TDNEGF, then injected spin polarized current (z-spin polarization in this case) will create z-spin polarization at weakly coupled sites 2, 4, 7, 9 as we see in the figure above and previous case of Fig. 9. Since, QSL spin is not being coupled back to TDNEGF in this particular case, electron spin density dynamics should remain unaffected by QSL. Here $J_{sd} = -0.3$ eV. Increasing strength of J_{sd} will result in more torque with higher magnitude of spin polarization on weakly coupled sites.

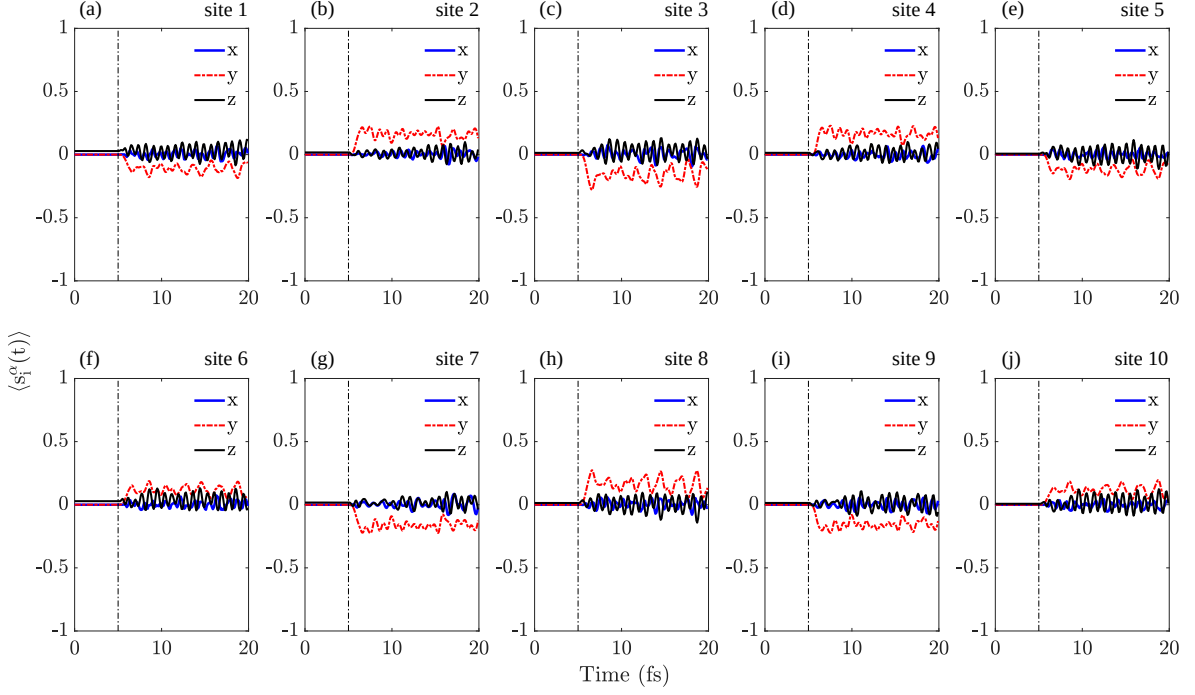


FIG. 29. Repeated the above analysis for higher J_{sd} i.e. $J_{sd} = -0.5$ eV. Local electron spin density is coupled with feedback to QSL (Az phase) at $t = 5$ fs (shown as dashed line). Here, $T = 50$ K, bias = 0.05 eV

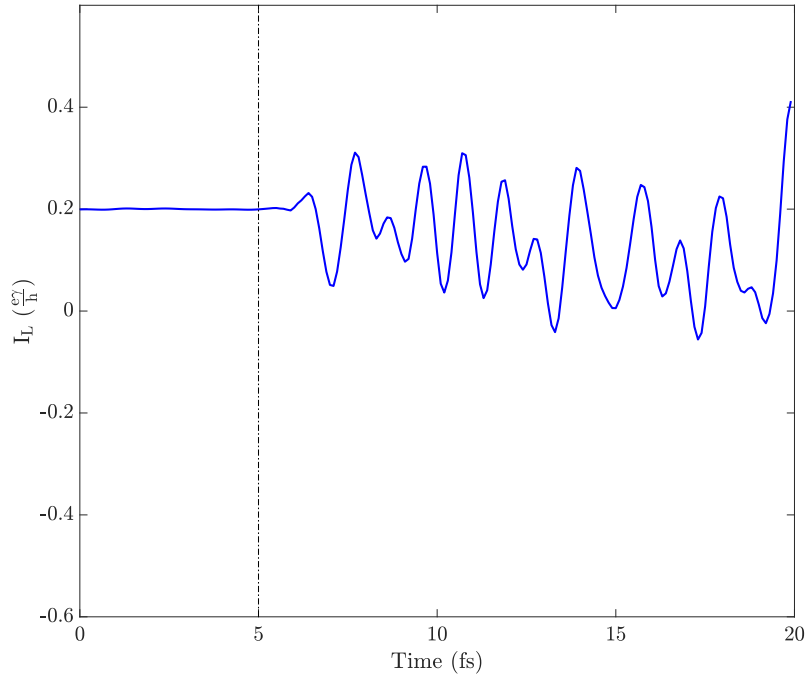


FIG. 30. Charge current dynamics as TDNEGF is coupled with QSL in A_z phase with feedback.

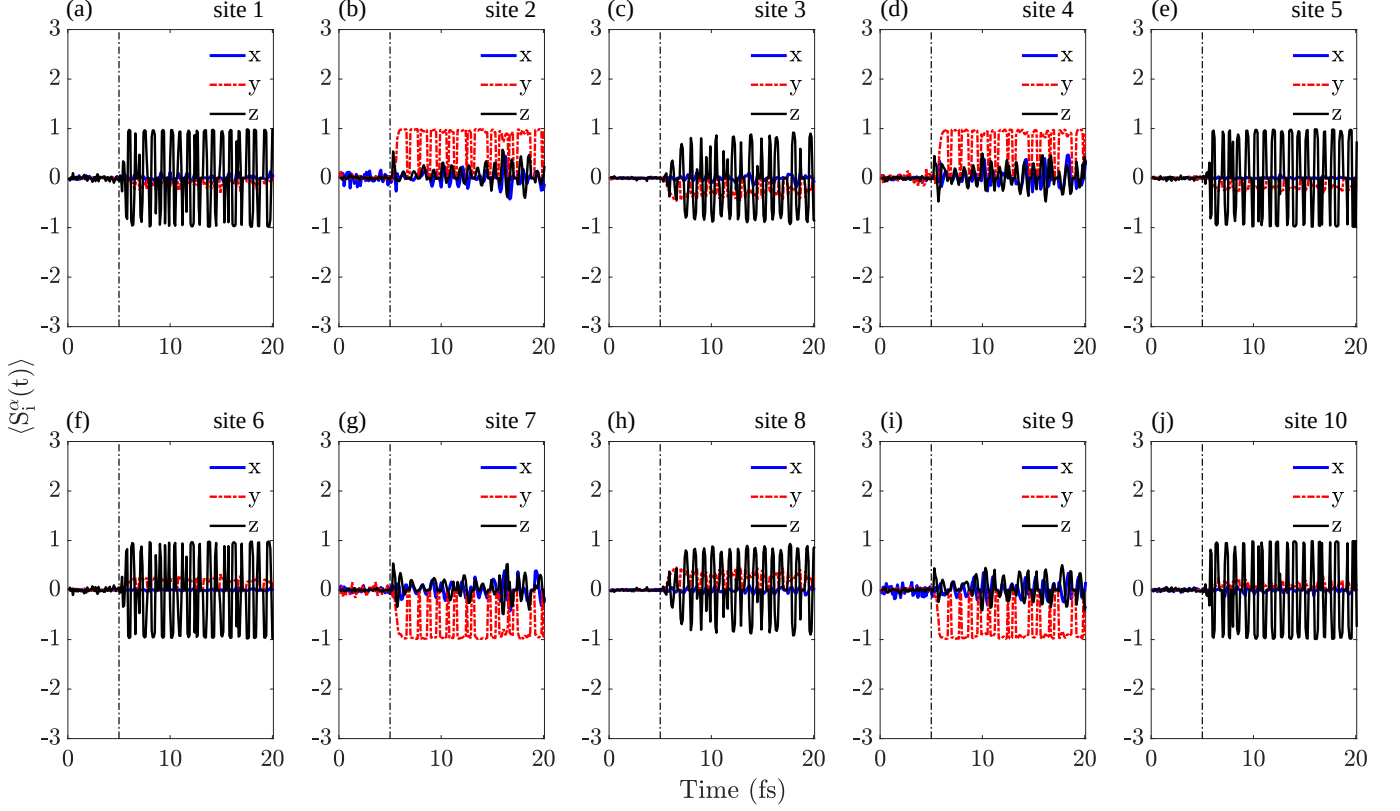


FIG. 31. Local spin dynamics (Kitaev QSL) due to feedback switched on after $t = 5 \text{ fs}$ (shown with dashed black line), $J_{sd} = -0.5 \text{ eV}$, bias = 0.05 eV. The overall dynamics is similar to that of $J_{sd} = -0.3 \text{ eV}$. The temperature here is $T = 50 \text{ K}$.

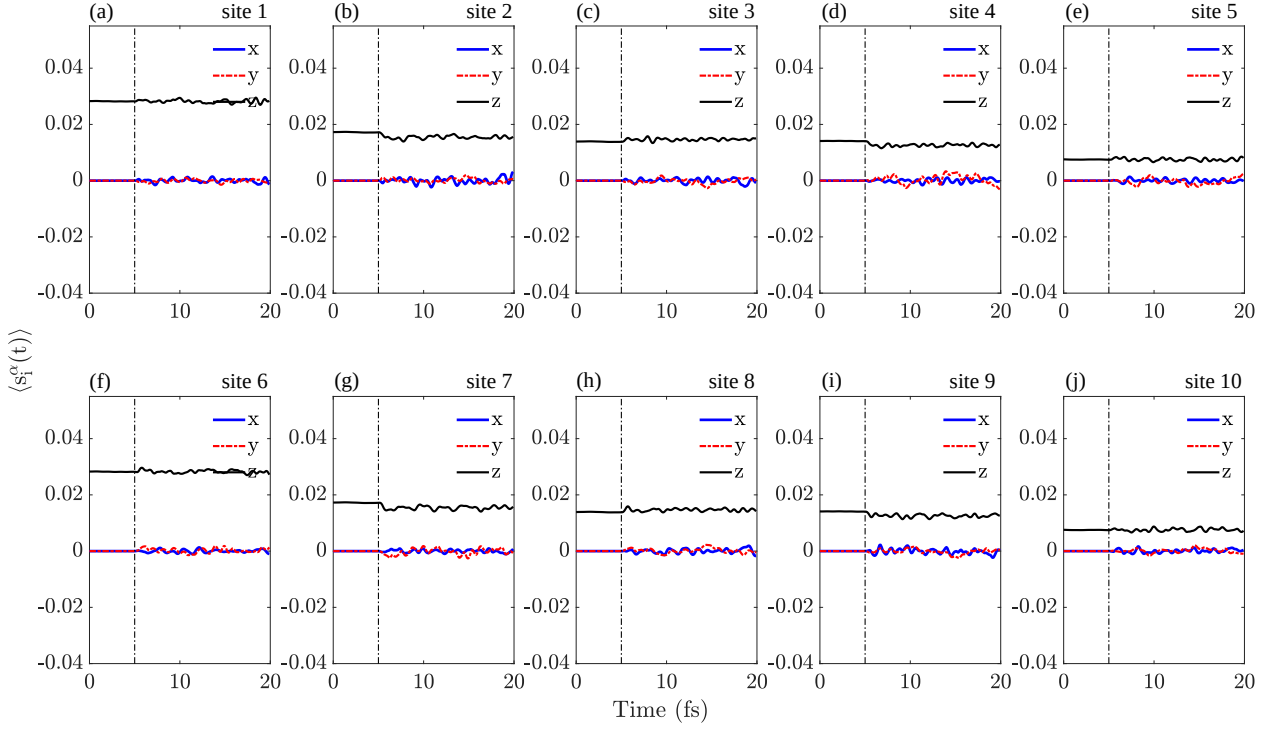


FIG. 32. Repeated the above analysis for smaller J_{sd} i.e. $J_{sd} = -0.1$ eV. We do see some fluctuation in local electron spin density dynamics as feedback coupling is switched on after $t = 5$ fs which is different than what was observed for $J_{sd} = -0.3$ or -0.5 eV case. The local electron spin density remains z-spin polarized (black) with small fluctuation in x-, y- components (blue, red). The applied bias is 0.05 eV, Temperature 50 K.

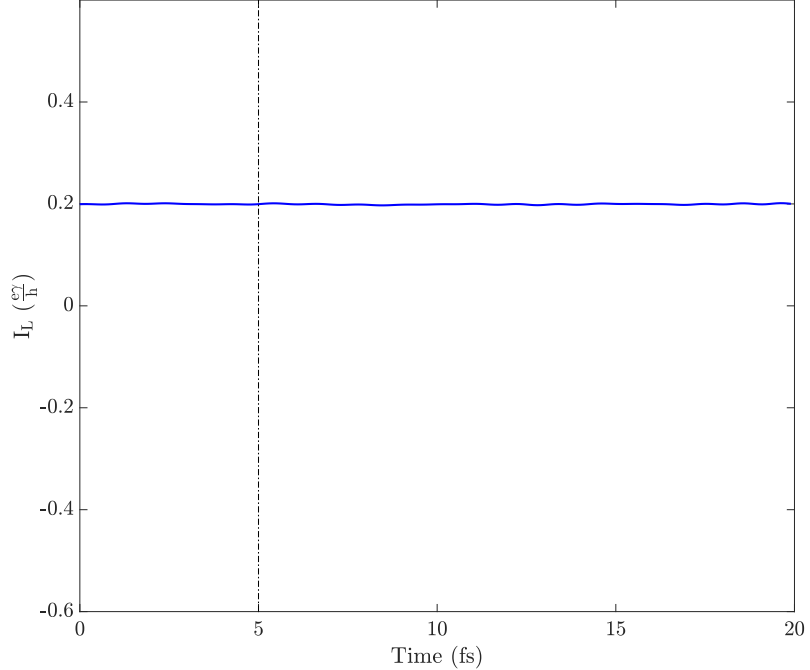


FIG. 33. Charge current dynamics as TDNEGF is coupled with QSL in A_z phase with feedback. Since, $J_{sd} = -0.1$ eV is small here, the effect of feedback coupling is too small to be detected in charge current dynamics. The feedback coupling is switched on after $t = 5$ fs.

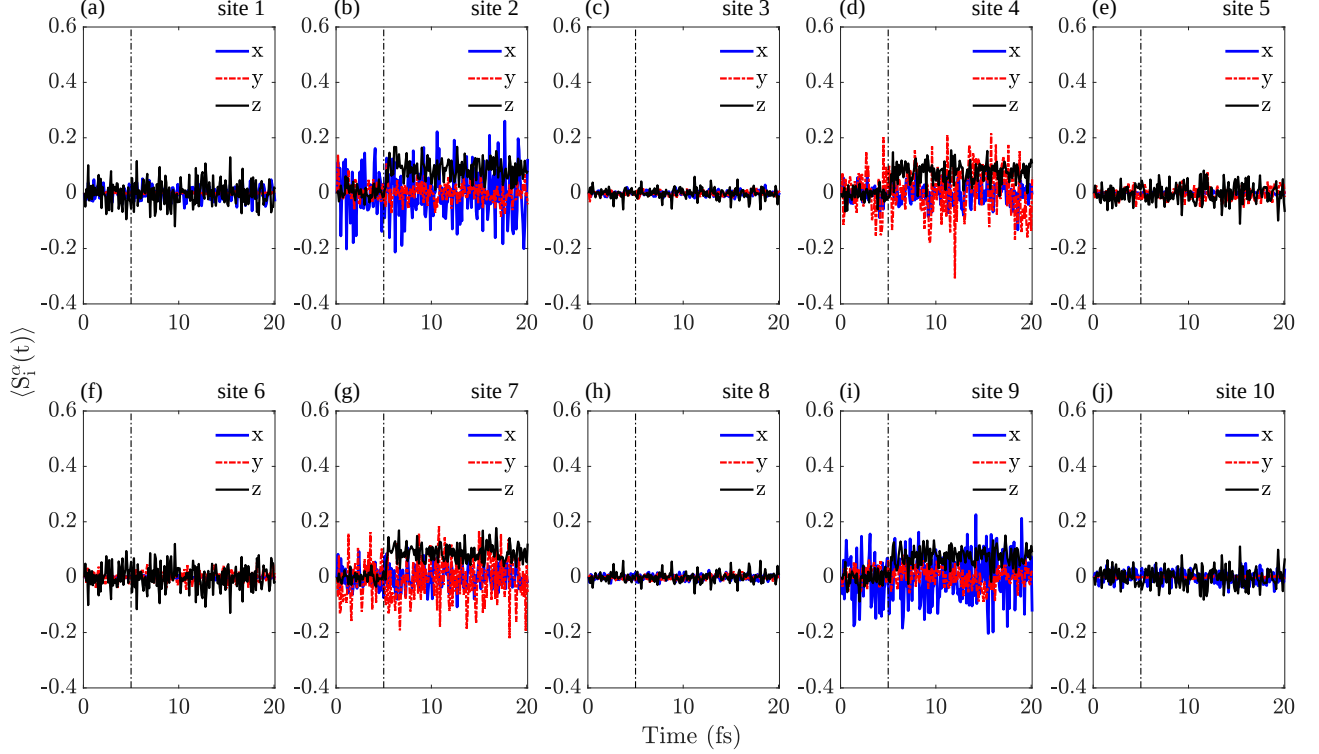


FIG. 34. The local spin dynamics (Kitaev QSL) is different for $J_{sd} = -0.1 \text{ eV}$ as one would expect intuitively by observing local electron spin density dynamics shown earlier (Fig. 31). Since, J_{sd} is small, the feedback torque on electron is small which allows the injected z-spin polarized electron to stay z-spin polarized even after feedback coupling with QSL is switched on after $t = 5 \text{ fs}$. The feedback coupling therefore causes weakly coupled sites (i.e. site 2, 4, 7, 9) to develop small positive z-spin polarization. Here, applied bias is 0.05 eV , Temperature, T is 50 K .